Nanoscale

PAPER

View Article Online
View Journal | View Issue

Cite this: *Nanoscale*, 2024, **16**, 8950

Coaxial dual-path electrochemical biosensing and logic strategy-based detection of lung cancer-derived exosomal PD-L1†

Junqiu Liu,[a] Zhaidong Liu,[b] Chunqin Zhao,[a] Yuting Jiao,[a] Baohong Li,[a] Jiaju Shi,[d] Zichao Chen*[c] and Zhen Zhang *[a]

Received 28th January 2024,
Accepted 2nd April 2024

DOI: 10.1039/d4nr00412d

rsc.li/nanoscale

Exosomal programmed death ligand-1 (ExoPD-L1) is a vital marker of immune activation in the early stages of tumor therapy and it can inhibit anti-tumor immune responses. However, due to the low expression of ExoPD-L1 in cancer cells, it is difficult to perform highly sensitive assays and accurately differentiate cancer sources. Therefore, we constructed a coaxial dual-path electrochemical biosensor for highly accurate identification and detection of ExoPD-L1 from lung cancer based on chemical–biological coaxial nanomaterials and nucleic acid molecular signal amplification strategies. The measurements showed that the detected ExoPD-L1 concentrations ranged from 6×10^2 particles per mL to 6×10^8 particles per mL, and the detection limit was 310 particles per mL. Compared to other sensors, the electrochemical biosensor designed in this study has a lower detection limit and a wider detection range. Furthermore, we also successfully identified lung cancer-derived ExoPD-L1 by analyzing multiple protein biomarkers expressed on exosomes through the "AND" logic strategy. This sensor platform is expected to realize highly sensitive detection and accurate analysis of multiple sources of ExoPD-L1 and provide ideas for the clinical detection of ExoPD-L1.

1. Introduction

Exosomal programmed death ligand-1 (ExoPD-L1) promotes the developmental process of cancer and is an important marker for cancer immunotherapy. ExoPD-L1 plays a key role in immunotherapy for many cancers, including lung cancer.[1,2] Therefore, the detection and identification of lung cancer-derived ExoPD-L1 is crucial for the treatment of lung cancer.[3–5] However, the existing methods not only lack sufficient sensitivity but also cannot effectively identify the cancer origin of ExoPD-L1 due to the content of lung cancer ExoPD-L1 being very low in human blood. Therefore, there is an urgent need to develop a novel sensor for highly sensitive detection and highly accurate identification of lung cancer-derived ExoPD-L1.

Compared with traditional detection methods such as fluorescence, the use of electrochemical biosensors has gained widespread attention in marker detection due to their high sensitivity and ease of operation,[6,7] but they still face challenges in the detection of low abundance ExoPD-L1. Advances in nanotechnology have enabled nanomaterials to show outstanding advantages in highly sensitive detection of electrochemical biosensors.[8–12] Nanomaterials can increase the active sites on the electrode surface and enhance the electron transfer rate, which improves the sensitivity and response speed of the sensor. Nucleic acid aptamers as probes are highly specific for the target molecule, enabling selective detection of the target.[13–17] DNA rolling ring replication (RCR), an isothermal amplification method for detecting DNA signals,[18–22] can further improve the specificity and sensitivity of electrochemical biosensors. Therefore, the development of novel electrochemical biosensors that integrate nanomaterials and the nucleic acid signal amplification strategy is expected to realize high specificity and sensitivity analysis of lung cancer-derived ExoPD-L1.

Hence, we constructed a coaxial dual-path electrochemical biosensor combining nanopillar bioprobes for electrocatalytic signal enhancement and DNA RCR amplification reaction for

[a]*Innovation Research Institute of Traditional Chinese Medicine, Shandong University of Traditional Chinese Medicine, Jinan, 250355, China. E-mail: zhangzhen19801981@126.com*
[b]*Affiliated Hospital of Shandong University of Traditional Chinese Medicine, Jinan, 250355, China*
[c]*Experimental Center, Shandong University of Traditional Chinese Medicine, Jinan, 250355, China. E-mail: chenzichao11@126.com*
[d]*School of Materials Science and Engineering, Sun Yat-sen University, Guangzhou 510275, China*

†Electronic supplementary information (ESI) available. See DOI: https://doi.org/10.1039/d4nr00412d

highly accurate recognition and detection of lung cancer ExoPD-L1 (Scheme 1). Firstly, nanopillar bioprobes were prepared using electrostatic spinning and DNA modification techniques. Secondly, the recognition-signal amplification probe H1H2 was modified on the electrodes to recognize ExoPD-L1 (H1) and trigger the RCR response (H2). Thirdly, the above recognition process and RCR reaction were triggered when ExoPD-L1 was present, and the nanopillar bioprobe combined with the rolled-ring programmed replication product to generate chemical–biological coaxial nanomaterials (CBCMs). Based on the programmed amplification of coaxial electrocatalytic nanomaterials (electron transfer capability), this achieves programmed enrichment enhancement of electrochemical signals. Finally, the constructed sensing strategy was logically analyzed to further identify the source of this exosome. Only when all three signals of ExoPD-L1, exosome marker proteins, and lung cancer marker proteins are output simultaneously, it can be indicated that the target is ExoPD-L1 derived from lung cancer, and then high-precision recognition and detection of lung cancer ExoPD-L1 are achieved. In addition, the electrochemical biosensor is universal and can detect ExoPD-L1 from different sources by specifically replacing the corresponding aptamer sequence.

2 Experimental section

2.1 Materials and reagents

Stannous chloride hydrate, polyvinylpyrrolidone (PVP, molecular weight: 1.3 million), 1-(3-dimethylaminopropyl)-3-ethylcarbodiimide hydrochloride (EDC), tris(2-carboxy-ethyl) phosphorus (TCEP), indium(III) nitrate hydrate, 6-mercapto-1-hexanol (MCH), streptavidin (SA), and thioglycolic acid (TA) were purchased from Aladdin (Shanghai, China). Potassium hexachloroplatinate and indium(III) acetate were ordered from Maclean Biochemical Co., Ltd (Shanghai, China). Phi29 DNA polymerase was ordered from Takara Biotechnology Co., Ltd (Dalian, China). The experimental reagents used were of analytical grade, and Millipore ultrapure water (≥18.25 MΩ) was used throughout the experiments. DNA sequences and phosphate buffered saline (PBS) were purchased from Sangon Biotech Co., Ltd (Shanghai, China).

2.2 Instruments

Transmission electron microscopy (TEM, JEOLJEM-2100) provided TEM images and energy dispersive X-ray spectroscopy (EDX) spectral data. The zeta potential was measured using Nano ZS90 (Malvern, USA). A saturated calomel electrode

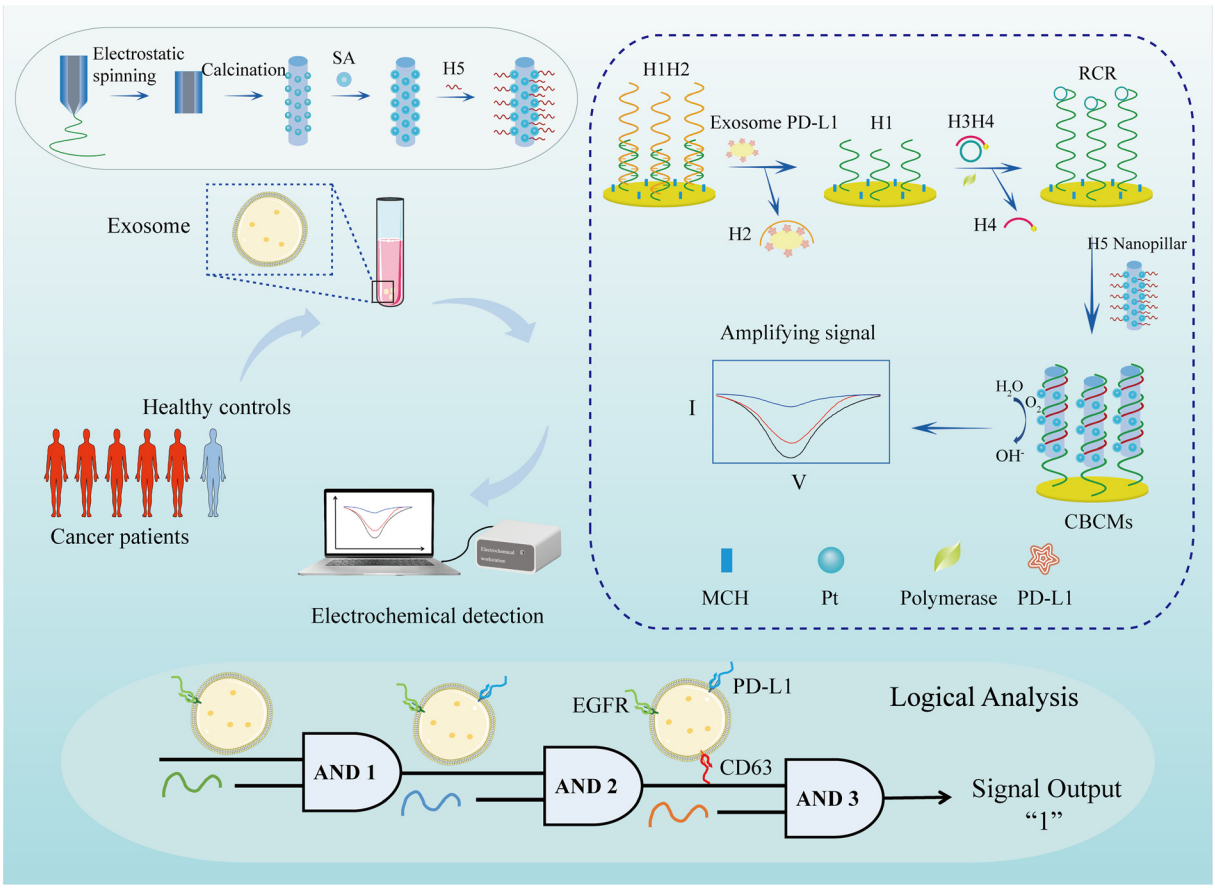

Scheme 1 Schematic illustration of the construction of coaxial dual-path electrochemical biosensor for highly accurate recognition and detection of lung cancer-derived ExoPD-L1.

(Shanghai Yidian Scientific Instrument Co., Ltd) was used as the reference electrode, a platinum electrode (Shanghai Yidian Scientific Instrument Co., Ltd) was used as the auxiliary electrode, and a gold electrode modified with functional nucleic acid sequences was used as the working electrode in the detection system. All measurements of nanopillar-based cyclic voltammetry (CV), differential pulse voltammetry (DPV) and electrochemical impedance spectroscopy (EIS) were carried out on a CHI660E electrochemical analyzer (manufactured by Shanghai Chenhua Instrument Co., Ltd) at room temperature. Cells were cultured in a carbon dioxide incubator (Thermo Forma, USA) and observed using an inverted fluorescence microscope (Olympus, JPN). Exosomes were extracted using an ultra-high-speed centrifuge (Beckman, USA).

2.3 Preparation of indium tin oxide/Pt (ITO/Pt) nanopillars

3.815 g PVP, 0.221 g $SnCl_4{\cdot}5H_2O$ and 1.0 g $In(NO_3)_3$ were dissolved in 19.5 g DMF and stirred magnetically at 25 °C for 19–20 h to turn into a homogeneous and clear DMF sol (C_{PVP} = 15.56 wt%).[23–25] 3.815 g PVP and 0.912 g K_2PtCl_6 were dissolved in DMF and stirred magnetically at 25 °C for 19–20 h to obtain a homogeneous and clarified DMF sol (C_{PVP} = 15.56 wt%).[18,26] The electrospinning device was assembled precisely according to the specifications, and the two types of transparent solutes were transferred into two 5 mL transparent syringes. Before installing and commissioning the electrospinning machine, the two 5 mL capacity transparent syringes were placed into the electrically driven intelligent syringe pump, and the double-drive inline needle was connected to the electrospinning metal electrode. The receiving device consists of a tinfoil and a grounding iron plate with a fixed distance adjustment of 180 mm between the grounding iron plate and the dual-drive inline needle. The flow rate of electrospinning was set at 10 μL min^{-1} and the voltage of electrospinning was 17 kV (DMF sol). After spinning for 8–10 h, the electric smart syringe pump was stopped and the tin foil and electrospinning material were removed and placed in a 65 °C oven to dry for 16–18 h. The electrospinning material was removed and then transferred into a muffle furnace, which was heated up to 900 °C at a rate of 3 °C min^{-1}. Mechanical grinding was performed and ITO/Pt nanopillars were obtained after the mixture was calcined for 120 min, naturally cooled to 25 °C and removed.

2.4 Electrochemical characterization of ITO/Pt nanopillars

The working electrodes were polished with 0.1 cm and 0.03 cm of alumina powder in turn, followed by thorough rinsing with water and ethanol, respectively, and then subjected to ultrasonic treatment to remove their excess alumina. The electrodes were dried in a nitrogen environment before being decorated and tested. 2 mg of ITO/Pt nanopillars were added to 2 mL of ethanol and sonicated for 50–60 min to obtain ITO/Pt nanopillars (1 mg mL^{-1}). Electrochemical data were obtained by scanning in 0.1 M potassium hydroxide solution (oxygen saturated) at a scan rate of 100 mV s^{-1} in the range of −0.9 V–0.2 V for CV, DPV, *etc*.

2.5 Preparation of ITO/Pt-H5 nanopillars

3 mg ITO/Pt nanoparticles were equally disseminated in 1.5 mL TA aqueous solution (2 mM). The resultant mixed solution needs to be treated with an ultrasonic device for 15–16 h before being washed with water again to prepare the carboxylated ITO/Pt coaxial nanomaterials ITO/Pt-TA. ITO/Pt-TA was mixed uniformly with SA in 10 mM PBS (with 10 mM EDC). EDC acted as a carboxylated amine-reactive cross-linking agent in the preparation, which could promote the formation of amino bonds between ITO/Pt-TA and SA to obtain ITO/Pt-SA nanopillars. Finally, the ITO/Pt-SA nanopillars and H5 were dispersed in 10 mM PBS at a mass ratio of 1 : 5 and a solid–liquid ratio of 1 : 10, and reacted in a 37 °C oscillator for 2 h. The ITO/Pt-H5 nanopillars were successfully obtained by repeated washing and centrifugation with ultrapure water 3 times.

2.6 Fabrication of electrochemical biosensor

The electrodes were carefully polished twice with alumina powder, extensively cleaned twice with water and ethanol, subjected to ultrasonic treatment to remove excess alumina, and dried with nitrogen. The working electrode was subjected to redox cycling in a mixture of KCl (0.01 M) and H_2SO_4 (0.05 M) to activate the electrode for later modification. 10 μL of a solution containing 2 μM TCEP and 5 mM H1 sequence was taken and added dropwise to the surface of the working electrode over 17–20 h at 25 °C. TCEP was used to open disulfide bonds in the DNA sequence, form Au–S bonds on the Au working electrode, and modify the DNA sequence probe on the surface of the Au electrode. The electrode was then washed with PBS 3 times to remove the non-specific adsorbed DNA sequences, and then the modified Au working electrode was immersed in 1 mM MCH for 70 min to seal the surface. The working electrode was then rinsed with PBS and 10 μL H2 sequence (5 μM) was drop-coated on the modified electrode surface and reacted with a DNA probe for 200 min at 37 °C. The modified electrode was rinsed again 3 times with PBS, and the H3H4 sequence and Phi29 DNA polymerase were added to the buffer solution for the assay. The H3H4 sequence in the solution was allowed to undergo a DNA RCR reaction with the H1 sequence on the modified electrode in the presence of the ExoPD-L1 target. The modified electrode was again rinsed with PBS 3 times, and the ITO/Pt-RCR was obtained by incubating the reaction mixture with 5 mL of ITO/Pt-H5 dispersion in the assay solution for 60 min at 37 °C. After rinsing with PBS, the electrochemical signal of ExoPD-L1 was detected in O_2 saturated PBS (pH = 7.5, 100 mM).

2.7 Cell culture

Human non-small cell lung cancer (NSCLC) cells (A549), mouse melanoma cells (B16F10), human breast cancer cells (MDA-MB-231), human colorectal cancer cells (HCT116), mouse breast cancer cells (4T1) and human normal hepatocytes (LO2) were all obtained from the Chinese Academy of Sciences Cell Bank (Shanghai, China). These cells were cultured in a medium containing 10% fetal bovine serum

(Lonsera, China) and 1% penicillin/streptomycin (Beyotime, China), and cultured at 37 °C in a 5% carbon dioxide incubator. A549 and B16F10 cells were cultured with RMPI-1640 (Servicebio, China). MDA-MB-231, HCT116, 4T1, and LO2 cells were cultured with DMEM (Servicebio, China).

2.8 Exosome extraction and identification

A549 cell-derived exosomes were extracted using ultracentrifugation: (1) A549 cells were cultured in 100 mm diameter Petri dishes, and when the cells reached 70–80%, the culture medium was discarded, washed 3 times with PBS, 10% serum-free culture medium was added to continue the incubation for 24 h, and the supernatant was collected; (2) the supernatant was centrifuged at 300*g* for 10 min at 4 °C to remove A549 cells; the cell supernatant was collected and transferred to a new centrifuge tube; (3) the supernatant was centrifuged at 2000*g* for 15 min at 4 °C to remove dead cells, and the supernatant was collected; (4) the supernatant was centrifuged at 10 000*g* for 30 min to remove cellular debris, was filtered through a sterile 0.22 μm filter, and then transferred to an ultra-high-speed tube; (5) the supernatant was centrifuged at 100 000*g* for 80 min at 4 °C to obtain a supernatant of A549 cells. Ultra-high-speed centrifugation was performed for 80 min at 4 °C to obtain the heteroprotein and exosome precipitates; and (6) the precipitates were resuspended in PBS at 4 °C, and centrifuged again at 100 000*g* for 80 min at 4 °C to remove the heteroproteins. Finally, the exosome precipitate was resuspended in PBS and stored at −80 °C.

Exosomes were characterized by transmission electron microscopy (TEM). In detail: (1) 10 μL of exosome dispersion was added onto a copper mesh, and the mesh was allowed to stand at room temperature for 15 min; (2) excess liquid was removed from the side of the mesh with filter paper, 10 μL of 2% phosphotungstic acid (pH = 6.5) was added onto the copper mesh and the mesh was negatively stained at room temperature for 1–2 min; (3) excess staining liquid was removed with filter paper, and the copper mesh was dried at room temperature; and (4) the morphology and number of exosomes were observed under a transmission electron microscope, at a 120 kV observation voltage.

2.9 Western blot verifies the expression of relevant proteins

The extracted exosomes were lysed with RIPA lysis buffer, the protein concentration of the samples was determined by using Nanodrop lite, and denaturation was carried out with 1× loading buffer at 100 °C for 5 min. Equal amounts of sample proteins were separated by electrophoresis using 10% SDS-PAGE, and then transferred to a PVDF membrane. After transferring the membrane for 0.5 h, the PVDF membrane was closed with 5% skimmed milk for 2 h. The primary antibody was then incubated at 4 °C overnight. The non-specific binding of the primary antibody was washed away with Tris-buffered saline Tween-20 (TBST) and the membrane was incubated with the secondary antibody for 1 h at room temperature. The non-specifically bound secondary antibody was also eluted with TBST and protein bands were detected using a multicolor fluorescence imaging system.

3 Results and discussion

3.1 Design of the coaxial dual-path electrochemical biosensor for ExoPD-L1

In this study, a coaxial dual-path electrochemical biosensor for ExoPD-L1 in lung cancer was constructed based on the synergistic strategy between the signal amplification capability of RCR products and catalytic properties of nanopillars. The catalytic signal amplifier was used as a multifunctional amplification platform to convert the target recognition information into electrochemical signals by using ExoPD-L1 as a target molecule, which successfully achieved highly sensitive detection for low-abundance ExoPD-L1, and further combined with the "AND" logic strategy to realize highly accurate analysis of ExoPD-L1 in lung cancer.

The specific mechanism is as follows: ITO/Pt nanopillars were prepared by using electrospinning technology. The surface of the nanopillars was modified with the nucleic acid sequence H5 through the biotin–streptavidin interaction, resulting in the formation of ITO/Pt-H5 nanopillar bioprobes. By utilizing the Au–S bond interaction, the H1 sequence was modified on the surface of the Au electrode. Subsequently, H2 was further hybridized onto the electrode. When the target ExoPD-L1 is present, H2 specifically binds to it and detaches from the electrode, thereby exposing H1. Subsequently, triggering the hybridization between H1 and the loop H3H4, H4 with a 3′-NH_2 blocking group detaches from the H3H4 loop. In the presence of Phi29 DNA polymerase, H4 stimulates H1 and H3 to undergo RCR reaction, generating amplified products. Finally, the ITO/Pt-H5 nanopillar signal probe with excellent electrocatalytic performance hybridizes with the RCR products on the electrode, achieving signal conversion and enrichment amplification, significantly improving the sensitivity of ExoPD-L1 detection. Furthermore, the source of exosomes was further determined by combining the "AND" logic strategy. For specific detection, H2 was replaced by sequence H6 recognizing the exosome marker protein CD63 and H7 recognizing the lung cancer marker protein EGFR. When all three exhibit signal output simultaneously, it can be proved that the target is ExoPD-L1 derived from lung cancer, achieving high-precision recognition and detection of ExoPD-L1.

CBCMs were prepared using chemical nanomaterials and nucleic acid aptamers. The self-assembly of CBCMs (ITO/Pt-RCR) was successfully realized by forming a coaxial conformational material with Pt-RCR products as the outer axes and ITO nanopillars as the inner axes. The CBCMs were generated *in situ* on a single electrode, and, as a three-dimensional sensing bio-amplifier, the CBCMs have superior electron transfer capability and biostability.

3.2 Characterization of the ITO/Pt nanopillars and exosomes

ITO/Pt nanopillars were successfully prepared based on the electrostatic spinning technique and characterized by scanning electron microscopy (Fig. 1A) and transmission electron microscopy (Fig. 1B and C) with an average diameter of about 180 nm. Experimental data showed that Pt nanoparticles

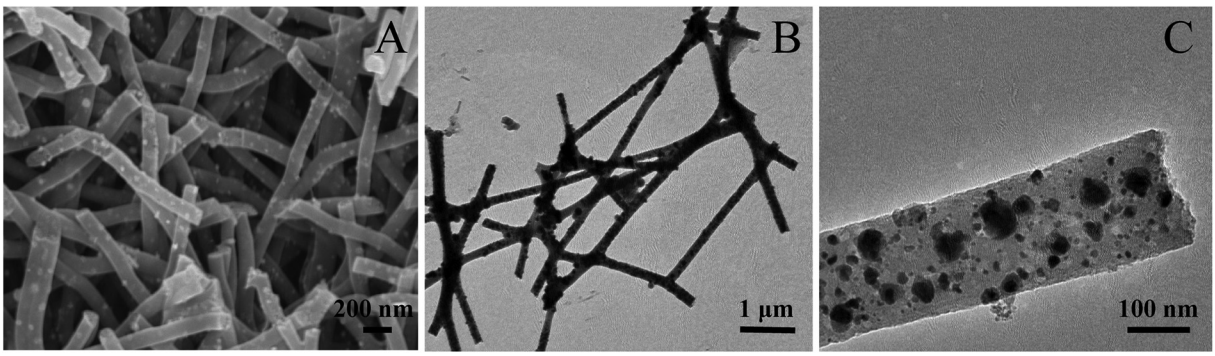

Fig. 1 Morphological characterization images of ITO/Pt nanopillars. (A) SEM image of ITO/Pt nanopillars. (B) TEM image of ITO/Pt nanopillars. (C) TEM magnification of ITO/Pt nanopillars.

formed ordered dot-like nanoconfigurations in the outer layer of the ITO nanopillars by the electrospinning stacking technique. Exosomes of lung cancer origin were extracted and isolated by differential centrifugation (Fig. 2A), and transmission electron microscopy was used to characterize the exosomes (Fig. 2B and C), with particle sizes ranging from 50 to 150 nm. The exosome marker proteins, CD63 and TSG101, were validated by western blot experiments (Fig. 2D). The expression of PD-L1 on exosomes was also verified (Fig. 2D).

The analysis of the target ExoPD-L1 protein was performed by 1.0% agarose gel electrophoresis and ethidium bromide (EB) staining activated the DNA RCR (Fig. 3A), providing effective technical support for the production of ITO/Pt-RCR (CBCMs). As shown in Fig. 3B, the zeta potential was characterized for ITO/Pt, ITO/Pt-TA, ITO/Pt-SA, ITO/Pt-H5 and ITO/Pt-RCR, respectively, and the experimental data showed that the CBCMs (ITO/Pt-RCR) were successfully achieved by self-assembly, with the Pt-RCR products as the outer axes and ITO nano-

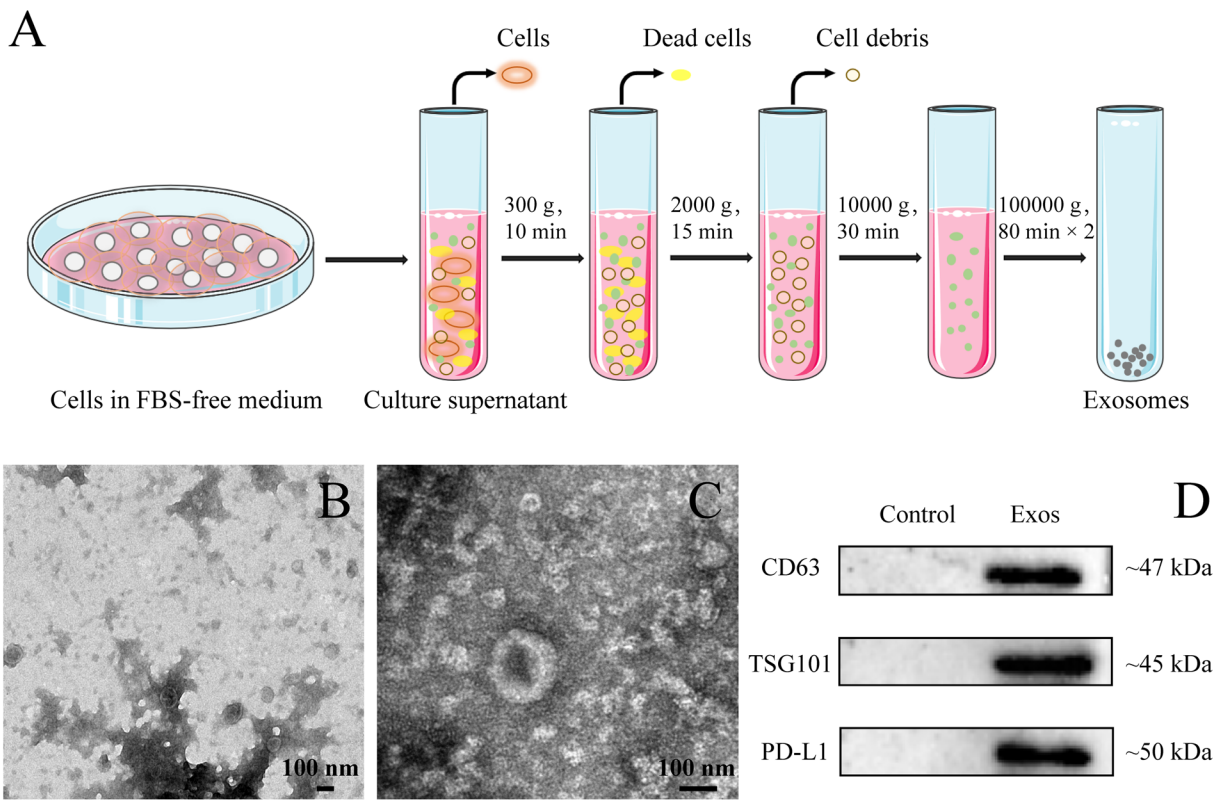

Fig. 2 Extraction steps and characterization of exosomes. (A) Steps of exosome extraction. (B and C) Transmission electron micrographs of lung cancer original exosomes. (D) Expression of exosome-related proteins.

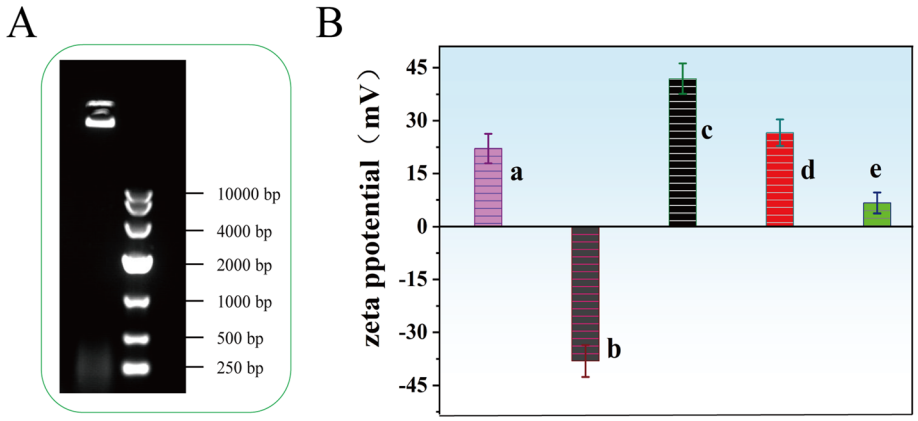

Fig. 3 (A) Agarose gel electrophoresis of the ITO/Pt-RCR product. (B) Zeta potential comparative analysis: (a) ITO/Pt nanoparticles, (b) ITO/Pt-TA, (c) ITO/Pt-SA, (d) ITO/Pt-H5, and (e) ITO/Pt-RCR.

pillars as the inner axes, forming a coaxial conformational material.

3.3 Electrochemical characterization of ITO/Pt nanopillars

The catalytic performance of the ITO/Pt nanopillars were characterized using electrochemical cyclic voltammetric curve experiments. Pt nanoparticle modified electrodes exhibit a clear reduction peak appearing at −0.43 V (Fig. 4A, curve a), while the reduction peak of the ITO/Pt nanopillars was significantly enhanced (Fig. 4A, curve b), indicating that ITO/Pt nanopillars have visible electrocatalytic activity. The electrochemical stability of the ITO/Pt coaxial nanopillars was verified using 100 CV cycles (10 mV s^{-1}) with a 0.1 M oxygen-saturated potassium hydroxide solution, and the experimental data showed that the change in the current density after 100 cycles was very small, which hardly affected the catalytic activity of the ITO/Pt nanopillars (Fig. 4B, curves a and b). In contrast to the ITO/Pt nanopillars (Fig. 4C, curve a), the CBCMs showed greater inter-

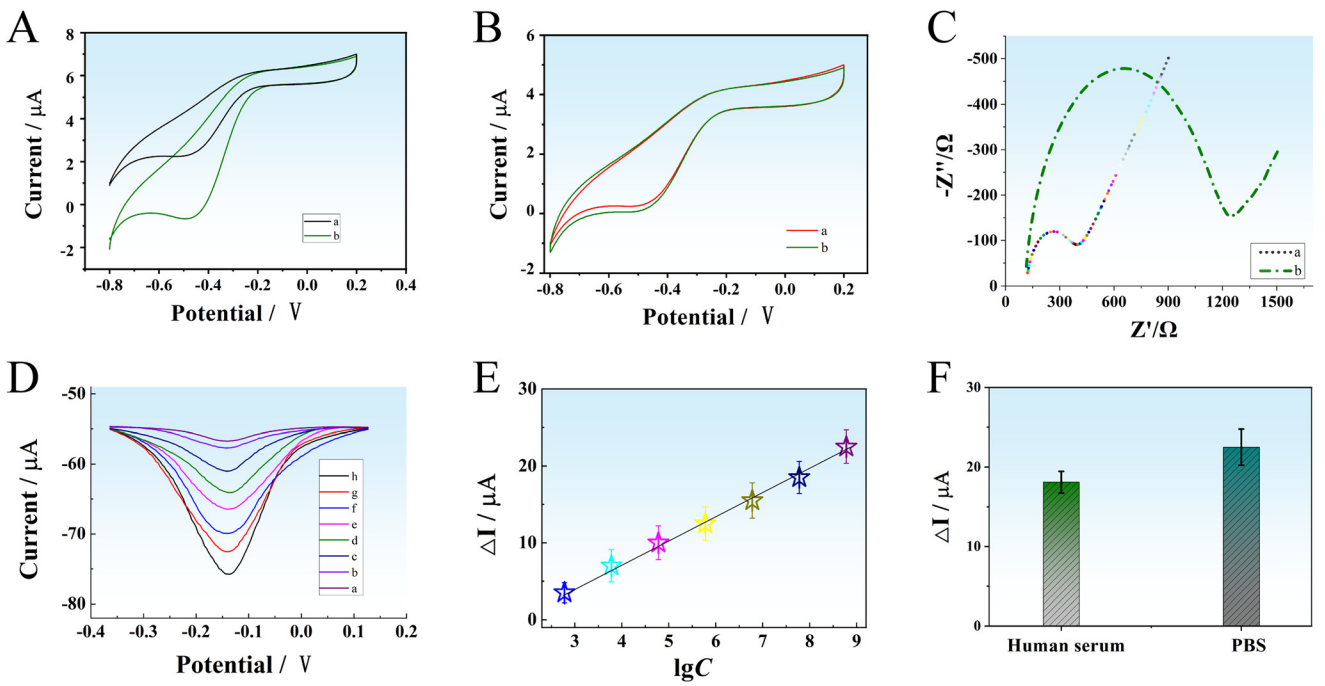

Fig. 4 Electrochemical characterization of ITO/Pt nanopillars. (A) Comparison of CV curves in 0.1 M oxygen-saturated KOH solution: (a) Pt nanoparticles and (b) ITO/Pt nanopillars. (B) CV curves of ITO/Pt nanopillars in 0.1 M KOH oxygen saturated solution. (C) EIS plots recorded in oxygen-saturated PBS (0.1 M, pH 7.6) for (a) ITO/Pt nanopillars and (b) CBCMs. (D) Changes in DPV responses to different concentrations of ExoPD-L1: (a–h) 0–6 × 10^8 particles per mL. (E) Corresponding calibration curves for ExoPD-L1 analysis. (F) Peak current intensity of ExoPD-L1 (6.0 × 10^5 particles per mL) detected by DPV curves in PBS and human serum. (Mean values of DPV curves were obtained from 3 replicate experiments with error bars as standard deviation of the 3 tests, and blanks were subtracted from each value.)

facial charge-transfer resistance (R_{ct}) (Fig. 4C, curve b), and the experimental data demonstrated that the RCR nucleic acid shells had been successfully modified on the surface of the ITO/Pt nanopillars.

3.4 Optimization of the experimental conditions of the biosensor

Polymerase is one of the important factors affecting the amplification of electrochemical sensing signals. On comparing the electrochemical signals of the Phi29 DNA polymerase dosage ranging from 0.2 U μL^{-1} to 0.7 U μL^{-1}, the results showed that 0.5 U μL^{-1} of polymerase was the optimal dose (Fig. S1†). The electrochemical signals of the chemical biosensor were evaluated under different temperature conditions (6.0×10^5 particles per mL, ExoPD-L1 protein of lung cancer origin), and the result showed that the optimal reaction temperature for obtaining the signals was 37 °C (Fig. S2†), so 37 °C was chosen as the reaction temperature for subsequent experiments.

In order to achieve the optimal performance of the chemical bioamplifier, the pH of ExoPD-L1 to be detected and the reaction time were compared experimentally. Fig. S3† demonstrates the effect of pH on the electrochemical reaction signal of DPV, and the optimal value of ΔI was obtained at pH = 7.5, so a buffer solution of pH = 7.5 was chosen for the subsequent experiments. Meanwhile, the reaction time is also one of the important factors affecting the biological activity of the enzyme and DNA hybridization. It was found that the incubation time had a positive correlation with the amplification signal, and the signal of the bioamplifier increased rapidly during the experiment, and reached the peak value after the experimental reaction reached 200 minutes (Fig. S4†). Based on this experimental result, 200 minutes should be chosen as the reaction time in subsequent experiments.

3.5 Analytical performance of the biosensor

To evaluate the analytical performance of this biosensor in detecting ExoPD-L1, the intensity variation of DPV peak currents was detected for different concentrations of lung cancer-derived ExoPD-L1 (0, 6×10^2, 6×10^3, 6×10^4, 6×10^5, 6×10^6, 6×10^7 and 6×10^8 particles per mL) after optimization of the reaction conditions. The constructed dual coaxial biosensor was capable of highly selective and sensitive detection of lung cancer ExoPD-L1 protein with a dynamic detection range of 6×10^2–6×10^8 particles per mL (Fig. 4D). Linear regression follows the equation $\Delta I = 3.066 \lg C - 4.944$ (Fig. 4E), the calibration curve has a correlation coefficient R^2 of 0.997 (3σ), and the detection limit is estimated to be 310 particles per mL (S/N = 3). The electrochemical biosensor has a lower detection limit and a wider detection range than other sensors (Table S2†). Fig. 4F shows that DPV marginally reduces the background signal in human serum in response to the ExoPD-L1 detection signal, whereas PBS does not, which may be due to interference from complex components in human serum.

The temporal stability of the sensor's DPV signal is also critical for clinical applications, and the DPV response of ExoPD-L1 remained above 95.7% over the 7-day test cycle. The repeatability of the sensor was tested using seven different par-

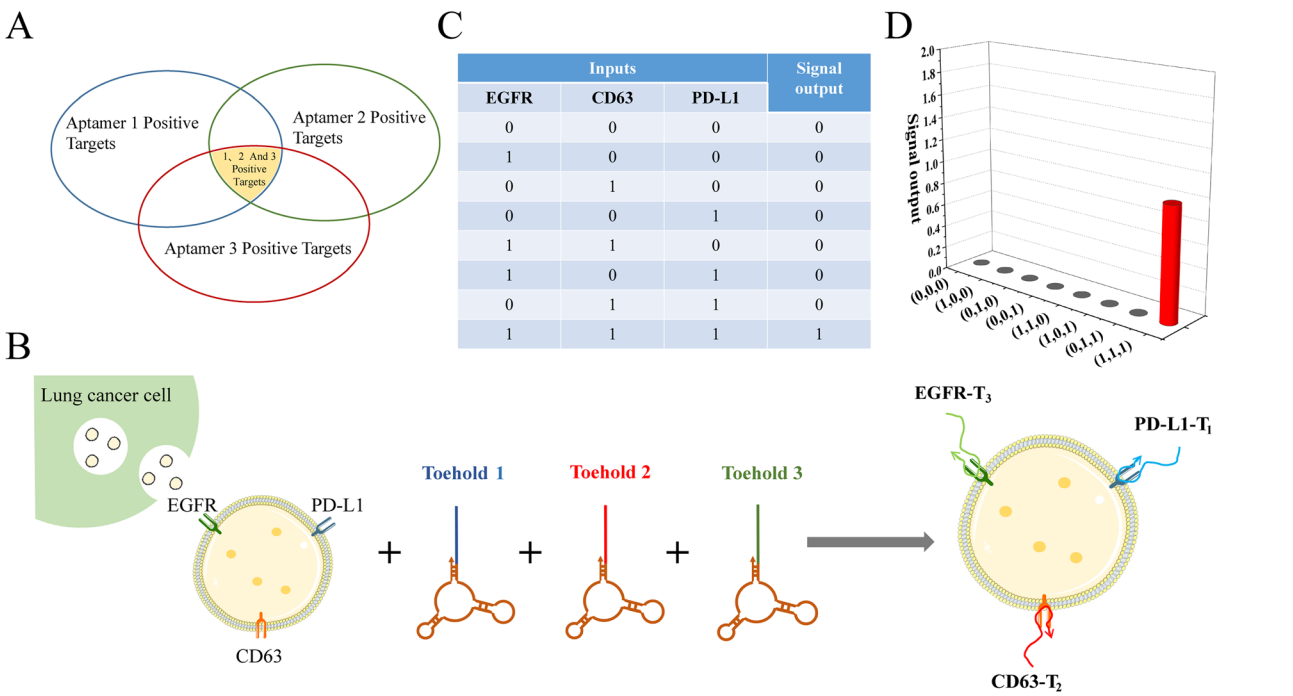

Fig. 5 Analysis of target identification based on the "AND" cascade logic strategy. (A) General principles of the three aptamer-based cellular recognition and separation logic device. (B) Activation mechanism of three aptamer binding targets. (C and D) Truth tables for the "AND" strategy. Signal output is only possible when EGFR, CD63, and PD-L1 are present at the same time.

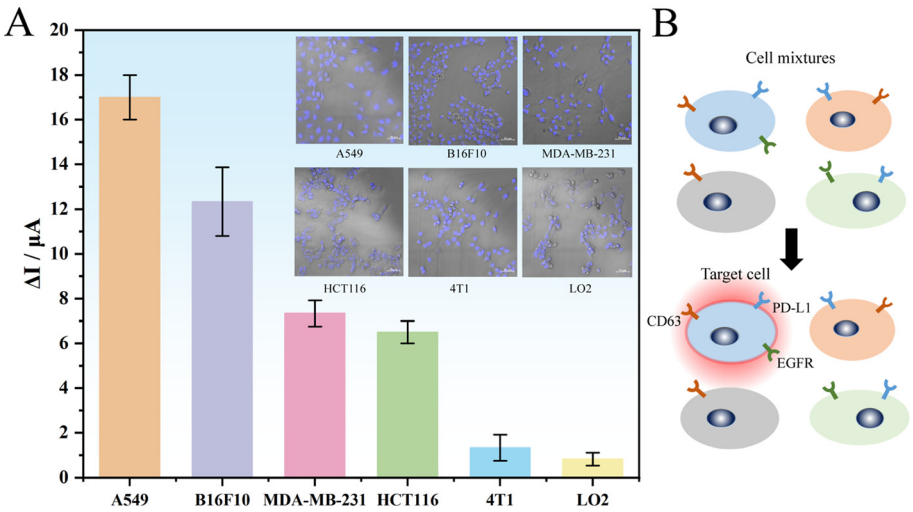

Fig. 6 Comparative tests on different cells. (A) Evaluation of coaxial electrochemical biosensor by different cells (inverted fluorescence microscopy to observe the cell morphology of A549, B16F10, MDA-MB-231, HCT116, 4T1 and LO2 cells). (B) Schematic diagram of precise identification of lung cancer-derived ExoPD-L1.

allel electrodes, and the calculated deviation was less than 6.2%. The results show that the electrochemical biosensor has good stability and repeatability. In order to investigate the selectivity of the developed sensor, we detected four common interfering substances in serum: ascorbic acid (AA), glucose (Glu), bovine serum albumin (BSA), and immunoglobulin (IgG). It can be seen that these four interfering substances do not significantly affect this electrochemical biosensor (Fig. S5†). The results confirmed the good specificity of the prepared sensor for ExoPD-L1.

3.6 Analysis of target identification based on the "AND" cascade logic strategy

It should be noted that to further confirm that the target is lung cancer ExoPD-L1, two additional probes, which recognize the lung cancer marker protein EGFR[27–29] and the exosome marker protein CD63, were added and analyzed by the "AND" logic strategy (Fig. 5A and B). Three independent variable inputs are defined as "1" when they are present and "0" when they are absent. An output signal will only be generated when all three are present, meaning they are all "1". At this point, the output signal is "1", confirming that the target is ExoPD-L1 derived from lung cancer. Based on the logical sequence of the cascade reaction, we obtained the truth value table shown in Fig. 5C and D.

3.7 Comparative experiments with different cells

In order to verify the selectivity of the experimental protocol, we also chose four tumor cells, B16F10, MDA-MB-231, HCT116, and 4T1, as well as exosomes secreted by LO2 from normal hepatocytes as a control group.[30–37] Under the same experimental conditions, the electrochemical signals of exosomes from these six cell sources were detected. As shown in Fig. 6A, the highest values of exosome electrochemical signals were obtained from A549 cells, followed by B16F10, MDA-MB-231, HCT116, and 4T1 cells, and the lowest values of exosome signals were obtained from LO2 cells. Analogous to the logic device in Fig. 5, the lung cancer marker protein EGFR was replaced with marker proteins of other cancers by introducing their corresponding aptamers, thus confirming that the target was ExoPD-L1 of the target cancer (Fig. 6B).

4 Conclusions

In conclusion, we constructed an electrochemical biosensor for high-precision detection of lung cancer ExoPD-L1, which utilized the excellent electrocatalytic properties of Pt-doped nanopillars and the DNA rolling circle replication amplification strategy to achieve highly sensitive detection of lung cancer ExoPD-L1 in the concentration range of 6×10^2 to 6×10^8 particles per mL. Meanwhile, accurate detection of lung cancer-derived ExoPD-L1 was achieved by logically analyzing multiple signature proteins on exosomes. In addition, the sensor is universal and can be used for the detection of ExoPD-L1 in more cancers by modifying the aptamers of other cancer marker proteins. We believe that this coaxial dual-path electrochemical biosensor construction idea is important for the high sensitivity and specificity detection of low-abundance ExoPD-L1, as well as the high-accuracy identification of cancer sources, and is expected to be used for the detection and analysis of more low-abundance biomarkers.

Author contributions

Junqiu Liu: conceptualization, methodology, investigation, writing – original draft, and visualization. Zhaidong Liu, Baohong Li and Jiaju Shi: software, methodology, formal ana-

lysis, and investigation. Chunqin Zhao and Yuting Jiao: formal analysis, supervision, and data curation. Zhen Zhang and Zichao Chen: conceptualization, methodology, formal analysis, project administration, writing – review & editing, funding acquisition, and supervision. All authors have given approval to the final version of the manuscript.

Conflicts of interest

The authors declare no conflict of interest.

Acknowledgements

This work was supported by the Taishan Scholar Foundation of Shandong Province (tsqn202211136), National Science Foundation of China (21775061), the Youth Talent Education Program of Shandong Universities (2021505031), the 20 Innovations Projects of Jinan Universities (202228085), and the Foundation of Innovative Research Teams of Accurate Disease Identification and Targeted Therapy (22202105).

References

1 D. H. Kim, H. Kim, Y. J. Choi, S. Y. Kim, J. E. Lee, K. J. Sung, Y. H. Sung, C. G. Pack, M. K. Jung, B. Han, K. Kim, W. S. Kim, S. J. Nam, C. M. Choi, M. Yun, J. C. Lee and J. K. Rho, *Exp. Mol. Med.*, 2019, **51**, 1–13.
2 J. Hu, Z. Mao, Y. Lu, Q. Chen, J. Xia, H. Deng and H. Chen, *Biosens. Bioelectron.*, 2023, **235**, 115379.
3 S. Akbar, A. Raza, R. Mohsin, A. Kanbour, S. Qadri, A. Parray, A. R. Zar Gul, A. Philip, S. Vijayakumar, M. Merhi, S. Hydrose, V. P. Inchakalody, R. Al-Abdulla, W. Abualainin, S. A. Sirriya, I. Al-Bozom, S. Uddin, O. M. Khan, M. I. Mohamed Ibrahim, U. Al Homsi and S. Dermime, *Front. Immunol.*, 2022, **13**, 1097117.
4 Y. Yang, H. Liu, Y. Chen, N. Xiao, Z. Zheng, H. Liu and J. Wan, *Cell Death Dis.*, 2023, **14**, 230.
5 Y. Cheng, F. Chang, Y. Gong and P. Lu, *Horm. Metab. Res.*, 2023, **55**, 788–793.
6 B. Wang, J. Hong, C. Liu, L. Zhu and L. Jiang, *Sensors*, 2021, **21**, 8240.
7 T. A. Enache, E. Matei and V. C. Diculescu, *Anal. Chem.*, 2019, **91**, 1920–1927.
8 X. Cao, N. Wang, S. Jia, L. Guo and K. Li, *Biosens. Bioelectron.*, 2013, **39**, 226–230.
9 T. Niazov, V. Pavlov, Y. Xiao, R. Gill and I. Willner, *Nano Lett.*, 2004, **4**, 1683–1687.
10 H. Li, W. Qiang, M. Vuki, D. Xu and H. Y. Chen, *Anal. Chem.*, 2011, **83**, 8945–8952.
11 J. K. Kim, K. J. Choi, M. Lee, M. H. Jo and S. Kim, *Biomaterials*, 2012, **33**, 207–217.
12 J. Li, F. Cheng, H. Huang, L. Li and J. J. Zhu, *Chem. Soc. Rev.*, 2015, **44**, 7855–7880.
13 B. T. Huang, W. Y. Lai, Y. C. Chang, J. W. Wang, S. D. Yeh, E. P. Lin and P. C. Yang, *Mol. Ther.–Nucleic Acids*, 2017, **8**, 520–528.
14 X. Xiong, H. Liu, Z. Zhao, M. B. Altman, D. Lopez-Colon, C. J. Yang, L. J. Chang, C. Liu and W. Tan, *Angew. Chem., Int. Ed.*, 2013, **52**, 1472–1476.
15 W. Y. Lai, B. T. Huang, J. W. Wang, P. Y. Lin and P. C. Yang, *Mol. Ther.–Nucleic Acids*, 2016, **5**, e397.
16 J. Chen, L. Zhang and R. Yu, *Food Chem.*, 2024, **442**, 138384.
17 X. Hu, H. Chi, X. Fu, J. Chen, L. Dong, S. Jiang, Y. Li, J. Chen, M. Cheng, Q. Min, Y. Tian and P. Zhang, *J. Am. Chem. Soc.*, 2024, **146**, 2514–2523.
18 Z. Zhang, M. Zhu, Z. Chen, X. Wang, G. Chen and S. Zhang, *Biosens. Bioelectron.*, 2019, **141**, 111414.
19 L. K. Limón, K. Shi, A. Dao, J. Rugloski, K. J. Tompkins, H. Aihara, W. R. Gordon and R. L. Evans, 3rd, *Acta Crystallogr., Sect. F: Struct. Biol. Commun.*, 2023, **79**, 295–300.
20 C. J. Harmer, F. Lebreton, J. Stam, P. T. McGann and R. M. Hall, *Microbiol. Spectrum*, 2022, **10**, e0228722.
21 M. Bonnamy, S. Blanc and Y. Michalakis, *mBio*, 2023, **14**, e0169223.
22 M. Jammes, V. Golyaev, A. Fuentes, N. Laboureau, C. Urbino, C. Plissonneau, M. Peterschmitt and M. M. Pooggin, *PLoS Pathog.*, 2024, **20**, e1011941.
23 M. Mierzwa, E. Lamouroux, I. Vakulko, P. Durand and M. Etienne, *Electrochim. Acta*, 2016, **202**, 55–65.
24 M. M. Munir, F. Iskandar, K. M. Yun, K. Okuyama and M. Abdullah, *Nanotechnology*, 2008, **19**, 145603.
25 M. M. Munir, H. Widiyandari, F. Iskandar and K. Okuyama, *Nanotechnology*, 2008, **19**, 375601.
26 M. Zhu, Z. Sun, Z. Zhang and S. Zhang, *Chem. Commun.*, 2018, **54**, 13431–13434.
27 F. K. Khalil and S. Altiok, *Cancer Control*, 2015, **22**, 193–199.
28 J. Codony-Servat, C. Codony-Servat, A. F. Cardona, A. Giménez-Capitán, A. Drozdowskyj, J. Berenguer, J. W. P. Bracht, M. Ito, N. Karachaliou and R. Rosell, *Clin. Lung Cancer*, 2019, **20**, 167–177.
29 S. Fang and Z. Wang, *Drug Des., Dev. Ther.*, 2014, **8**, 1595–1611.
30 C. Xie, X. Zhou, C. Liang, X. Li, M. Ge, Y. Chen, J. Yin, J. Zhu and C. Zhong, *J. Exp. Clin. Cancer Res.*, 2021, **40**, 266.
31 E. J. Choe, C. H. Lee, J. H. Bae, J. M. Park, S. S. Park and M. C. Baek, *Pharmaceutics*, 2022, **14**, 1660.
32 Z. Li, J. Zhou, J. Zhang, S. Li, H. Wang and J. Du, *Int. J. Cancer*, 2019, **145**, 1946–1957.
33 K. A. Schalper, D. Carvajal-Hausdorf, J. McLaughlin, M. Altan, V. Velcheti, P. Gaule, M. F. Sanmamed, L. Chen, R. S. Herbst and D. L. Rimm, *Clin. Cancer Res.*, 2017, **23**, 370–378.
34 N. M. Naba, N. Tolay, B. Erman and A. Sayi Yazgan, *Turk. J. Biol.*, 2020, **44**, 15–23.
35 G. Dong, X. Huang, R. Chen, L. Wu, S. Jiang and S. Chen, *Oxid. Med. Cell. Longevity*, 2022, **2022**, 5954437.

36 M. Bajor, A. Graczyk-Jarzynka, K. Marhelava, A. Burdzinska, A. Muchowicz, A. Goral, A. Zhylko, K. Soroczynska, K. Retecki, M. Krawczyk, M. Klopotowska, Z. Pilch, L. Paczek, K. J. Malmberg, S. Wälchli, M. Winiarska and R. Zagozdzon, *J. Immunother. Cancer*, 2022, **10**, e002500.

37 C. D'Alterio, M. Buoncervello, C. Ieranò, M. Napolitano, L. Portella, G. Rea, A. Barbieri, A. Luciano, G. Scognamiglio, F. Tatangelo, A. M. Anniciello, M. Monaco, E. Cavalcanti, P. Maiolino, G. Romagnoli, C. Arra, G. Botti, L. Gabriele and S. Scala, *J. Exp. Clin. Cancer Res.*, 2019, **38**, 432.